Proceedings of the 14th International Symposium Ultrafast Phenomena in Semiconductors, Vilnius 2010

Morphology and Magnetic Coupling in ZnO:Co and ZnO:Ni Co-Doped with Li

C. Persson[a,b,*], O.D. Jayakumar[c], C. Sudakar[d], V. Sudarsan[c] and A.K. Tyagi[c]

[a]Department of Materials Science and Engineering, Royal Institute of Technology, SE-100 44 Stockholm, Sweden

[b]Department of Physics, University of Oslo, P.O.Box 1048 Blindern, NO-0316 Oslo, Norway

[c]Chemistry Division, Bhabha Atomic Research Centre, Mumbai 400085, India

[d]Department of Physics and Astronomy, Wayne State University, Detroit, MI 48201, USA

$Zn_{0.95}Co_{0.05}O$ and $Zn_{0.97}Ni_{0.03}O$ nanorods, prepared by a solvothermal method, show intriguing morphology and magnetic properties when co-doped with Li. At low and moderate Li incorporation (below 10 and 3 at.% Li in the Co- and Ni-doped samples, respectively) the rod aspect ratio is increased and room temperature ferromagnetic properties are enhanced, whereas the ferromagnetic coupling in $Zn_{0.97}Ni_{0.03}O$ is decreased for Li concentrations > 3 at.%. First-principles theoretical analyses demonstrate that Li co-doping has primarily two effects in bulk $Zn_{1-x}M_xO$ (with M = Co or Ni). First, the Li-on-Zn acceptors increase the local magnetic moment by depopulating the M 3*d* minority spin-states. The magnetic coupling is Ruderman–Kittel–Kasuya–Yosida-like both without and with Li co-doping. Second, Li-on-Zn prefer to be close to the M atoms to compensate the M–O bonds and to locally depopulate the 3*d* states, and this will help forming high aspect nanostructures. The observed room temperature ferromagnetism in Li co-doped $Zn_{1-x}M_xO$ nanorods can therefore be explained by the better rod morphology in combination with ionizing the magnetic M atoms.

PACS: 71.20.Nr, 71.55.Gs, 75.50.−y

1. Introduction

Nanostructured ZnO have been suggested as active material in a broad range of high technology applications. Bulk ZnO is semiconductor with many material advantages for optoelectronics, for instance [1–3]: (i) large intrinsic energy band gap that easily can be tuned by doping. (ii) Excellent transparent *n*-type conducting properties. (iii) Large exciton binding energy. (iv) Native ZnO can generate white light luminescence. (v) Recent studies on vacancies in ZnO as well as studies on transition-metal doped ZnO indicate room temperature ferromagnetism (FM), thereby ZnO is being a potential candidate material in spintronic devices. However, FM phase in bulk ZnO is still under debate, see references in [4, 5].

In this paper we discuss our recent studies on morphology and magnetic properties in nanostructured $Zn_{1-x}M_xO$ with M = Co [6] and with M = Ni [7] co-doped with Li. We have experimentally found that Li co-doping of $Zn_{1-x}M_xO$ nanorods enhances both the rod morphology as well as the room temperature FM phase. We present first-principles modeling of bulk $Zn_{1-x}M_xO$ demonstrating that the total energies of the FM and the antiferromagnetic (AFM) phases are very comparable. Additional low and moderate Li-on-Zn co-doping increases the local magnetic moment mainly via depopulation of the Co and Ni 3*d*-states. The magnetic moment of bulk $Zn_{1-x}M_xO$ is the Ruderman–Kittel–Kasuya–Yosida-like (RKKY) both without and with additional Li-on-Zn acceptors. The total energy calculations cannot explain the room temperature FM phase. Instead, the main theoretical conclusion is that Li-on-Zn acceptors compensate the Co–O and Ni–O bonds, which can explain the better rod morphology. The room temperature FM phase in Li co-doped $Zn_{1-x}M_xO$ nanorod may thereby be explained by a better rod morphology in combination with depopulation of the Co and Ni 3*d*-states.

2. Experimental details

ZnO nanowires/rods were synthesized from zinc acetate dihydrate (10 mmol) (99.99%) which was mixed with 15 ml of trioctylamine in a round bottomed flask. The mixtures were rapidly heated to 320 °C and maintained at that temperature for 2 h with refluxing and cooled to room temperature. The white precipitate obtained was washed several times with acetone and absolute ethanol and dried by a roto-evaporator. The same procedure was followed to prepare $Zn_{1-x}M_xO$ co-doped with Li, by taking Co or Ni acetate in combination with Li acetate in the appropriate proportion. The phase purity and crystal structure of the samples were analyzed using a Philips diffractometer (model PW 1071) using

* corresponding author; e-mail: Clas.Persson@mse.kth.se

Cu K_α radiation fitted with graphite crystal monochromator. High-resolution transmission electron microscopy (HRTEM) imaging and selected area electron diffraction (SAED) studies were carried out with a JEOL JEM 2010 transmission electron microscope. DC magnetization measurements were carried out using an EG&G PAR vibrating sample magnetometer (model 4500).

3. Computational details

The $Zn_{1-x-y}M_xLi_yO$ compounds were modelled by a $3 \times 3 \times 2$ wurtzite-like bulk structure consisting of 72 atoms. Total energy was obtained from the first--principles projector augmented wave method [8] with the local spin density approximation (LSDA) in the Kohn–Sham equation, based on the density functional theory. Computational parameters were a $6 \times 6 \times 6$ Γ-centred $\boldsymbol{k}$-mesh and a 400 eV energy cut-off. Experimental lattice constants were used, and all ions are fully relaxed by means of both the conjugate-gradient and quasi--Newton algorithms with a $3 \times 3 \times 3$ $\boldsymbol{k}$-mesh. The convergence is 0.1 meV for the total energy of the unit cell and 8 meV/Å for the forces of each atom. Total and local magnetic moments, as well as spin-dependent and atom-resolved density-of-states (DOS) were obtained using the LSDA+U method described by a self-interaction--like Coulomb correction with U_d(Co; Ni) = 4 eV and U_d(Zn) = 6 eV. The correction of the Zn d orbitals within LSDA+U have been found [9, 10] to localize significantly the Zn $3d^{10}$-states, thereby improving the Zn-d–O-p hybridization at 7 eV below the valence-band maximum. The Coulomb correction of the Co and Ni d-states follows earlier studies on for instance CoO [11, 12] and similar transition-metals systems. To verify that the underestimated band gap does not affect the main conclusion, we have also performed complementary LSDA+U calculations with the additional Coulomb potential U_s(O) = −8 eV to correct the ZnO band gap [9, 13]. In the calculations, the Co and Ni concentration was fixed to either $x = 0$ or $1/32 \approx 3$ at.%. The variations in Li doping concentration were obtained by $y = 0$, 1/32, 2/32, and 3/32 in the $Zn_{31/32-y}M_{1/32}Li_yO$ supercell, thus ≈ 0, 3, 6, and 9 at.% Li.

4. Results

Pure ZnO samples (Fig. 1) show nanorod morphology having length around 0.5–3 μm with a diameter of around 100–150 nm (i.e., a high aspect ratio of 5–20). Incorporating M = Co or Ni reduces significantly the aspect ratio of the nanorods (≈ 1–5), turning into spherical-like irregular particles at 5 at.% Co or 3 at.% Ni. Thus, Co and Ni destabilize the rod shape of the ZnO nanostructures. Unlike Co and Ni dopant, adding 3–10 at.% Li in pure ZnO or in $Zn_{1-x}M_xO$ does not change the morphology of ZnO particles, and in fact it retains the nanorod shape with higher aspect ratio (≈ 15–30). Li co-doping thus helps to stabilize the nanorod shape of $Zn_{1-x}M_xO$ [5, 6].

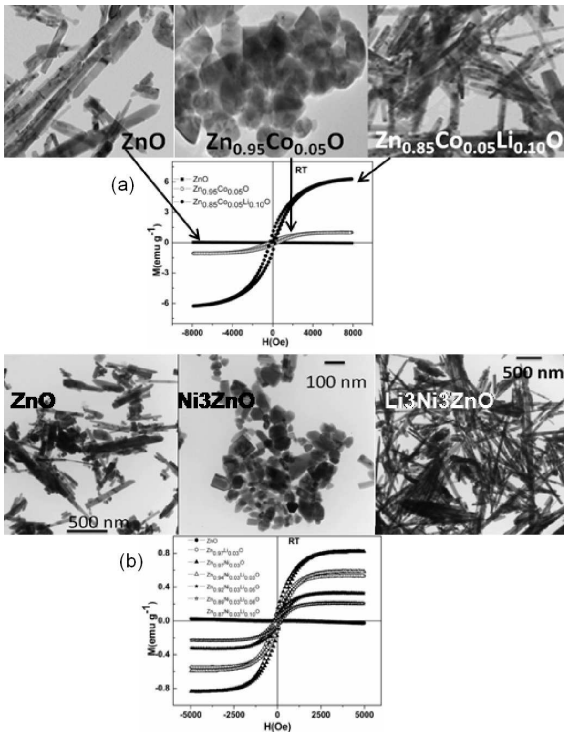

Fig. 1. (a) A simultaneous change in morphology and magnetic properties on mere Li-on-Zn substitution in $Zn_{0.95}Co_{0.05}O$ is seen by the TEM and magnetization studies. Li stabilizes the Co–O bonds, thereby improves both the morphology and magnetic properties of the nanorods. (b) Diamagnetic ZnO rods become room temperature FM particles on doping with 3 at.% Ni. On Li co-doping the $Zn_{0.97}Ni_{0.03}O$ with 3 at.% Li, the particles become rods with enhanced aspect ratio and the room temperature FM. Increasing Li concentration above 3 at.% decreases both the aspect ratio and the FM moment.

The room temperature DC magnetization loops for $Zn_{0.95-y}Co_{0.05}Li_yO$ (y = 0, 0.05, and 0.10) and $Zn_{0.97-y}Ni_{0.03}Li_yO$ (y = 0, 0.03, 0.05, 0.08, and 0.10) are depicted in Fig. 1. While pristine ZnO as well as Li-doped ZnO show a diamagnetic behavior, the $Zn_{1-x}M_xO$ nanorods show FM phase at 300 K. This magnetization is further increased by low or moderate Li incorporation. For instance, the $Zn_{0.97}Ni_{0.03}O$ sample has magnetic moment of 0.5 emu/g, and co-doped $Zn_{0.94}Ni_{0.03}Li_{0.03}O$ has increased value of 0.8 emu/g. However, very high Li concentrations decrease the magnetic moment: 0.2 emu/g for $Zn_{0.87}Ni_{0.03}Li_{0.10}O$.

The theoretical analyses on bulk $Zn_{0.94}M_{0.06}O$ (with M = Co or Ni) reveals that the local magnetic moment is 3.0 μ_B/Co and 2.0 μ_B/Ni as expected from the Co $3d^7$ and Ni $3d^8$ electron configurations. The AFM coupling is energetically favored for $Zn_{0.94}M_{0.06}O$, whereas FM coupling is favored for high Li co-doped $Zn_{0.94}M_{0.06}O$. However, the differences in the total energy and in the local magnetic moment of various FM and AFM crystalline configurations are very small (less than 50 meV

and 0.02 μ_B per M atom). This indicates paramagnetic phase of bulk $Zn_{0.94-y}M_{0.06}Li_yO$.

Moderate Li-incorporation of $Zn_{0.97}M_{0.03}O$ (filled marks in Fig. 2) increases the magnetic moment by 1.0 μ_B/Li-atom due to ionization of the M 3*d* minority--spin states. Maximum magnetic moment of 5.0 μ_B/Co occurs for $Zn_{0.91}Co_{0.03}Li_{0.06}O$ where Co has been ionized to Co $3d^5$. This is analogous to the Mn $3d^5$ which is known to generate a magnetic moment of 5.0 μ_B/Mn in ZnO:Mn [13]. Thus, the increase of the magnetic moment originates mainly from a local effect through depopulation of the transition metal 3*d* states. To demonstrate this, we present $Zn_{0.97}M_{0.03}O$ with additional hole doping (open marks in Fig. 2); negative values imply electron doping. At low and moderate hole doping, the magnetic moment follows the same linear trend as the Li-on-Zn acceptors with 5.0 μ_B/Co for $Zn_{0.97}Co_{0.03}O$ with 6% holes.

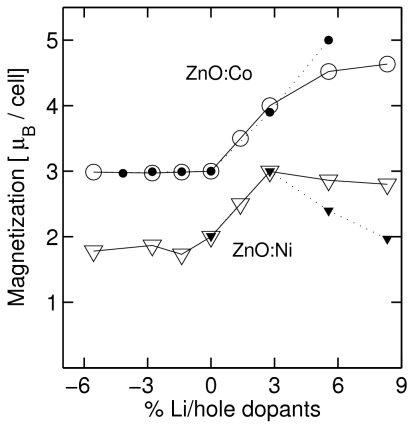

Fig. 2. Calculated total magnetic moment of the 72--atom supercells $Zn_{31/32-y}Co_{1/32}Li_yO$ (filled circles), $Zn_{31/32-y}Ni_{1/32}Li_yO$ (filled rectangles) as function of Li-on-Zn acceptor content $y = 0$, 1/32, and 2/32, thus about 0, 3, and 6 at.% Li, respectively. Open circles and rectangles show corresponding $Zn_{31/32}Co_{1/32}O$ and $Zn_{31/32}Ni_{1/32}O$ as function of additional free-hole doping (negative numbers imply free-electron doping). For moderate Li content, the Li-on-Zn acceptors act thus primarily as free-hole dopants.

To understand why the magnetic moment of hole--doped $Zn_{0.97}M_{0.03}O$ does not follow a linear trend for very high hole concentration, and also to understand why hole-doped $Zn_{0.97}Co_{0.03}O$ has a larger maximum magnetic moment compared with $Zn_{0.97}Ni_{0.03}O$, one has to study the spin-resolved DOS (Fig. 3). Low hole concentrations depopulate the energetically highest M 3*d* states that are above the valence-band maximum of host ZnO. Thereby the Fermi level lowers. At sufficient high hole concentrations, the Fermi level lowers below this valence--band maximum. Then it is mainly the host ZnO that becomes depopulated instead of the M 3*d* states. At this stage one could expect a hole mediated FM coupling, however we find no such magnetic phase in our configuration of the M sublattice. The depopulation of the host ZnO does generate a magnetic moment of the O *p*--like states, however all oxygens are magnetically induced (0.15–0.20 μ_B/O for O closest to Ni and $\approx$ 0.01 μ_B/O for the other O in $Zn_{0.97}Ni_{0.03}O$ with 6% holes) and their magnetic moments are orientated in order to stabilize and even decrease the total magnetic moment (Fig. 2). This induced magnetization of surrounding oxygens at high Li concentrations enhances thus a paramagnetic phase. Furthermore, the reason why the maximum magnetic moment can reach 5.0 μ_B/Co in hole-doped $Zn_{0.97}Co_{0.03}O$ whereas only 3.0 μ_B/Ni in $Zn_{0.97}Ni_{0.03}O$ is that the Co 3*d* states are energetically less localized (higher in energy) compared with the Ni 3*d* states (Fig. 3). It requires therefore higher hole concentrations in $Zn_{0.97}Co_{0.03}O$ (compared with $Zn_{0.97}Ni_{0.03}O$) to reach ZnO valence-band maximum, and the stronger ionization of the Co 3*d* implies a larger local magnetic moment.

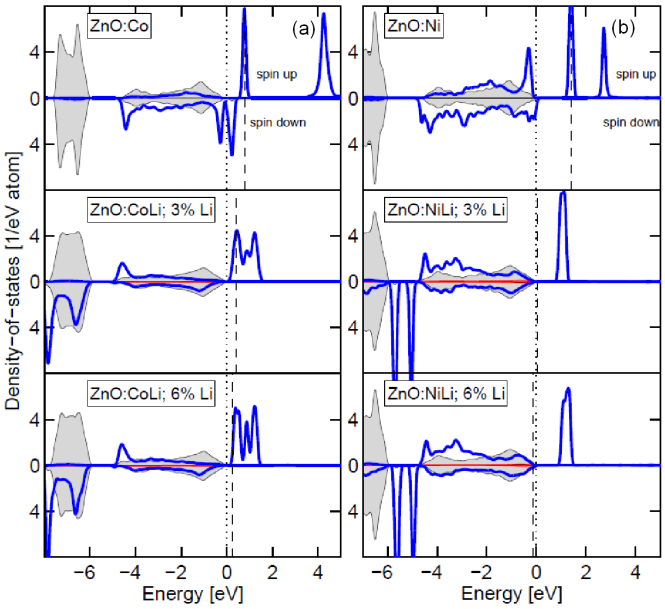

Fig. 3. Spin-dependent partial DOS of (a) $Zn_{31/32-y}Co_{1/32}Li_yO$ and (b) $Zn_{31/32-y}Ni_{1/32}Li_yO$ with $y = 0$, 1/32, and 2/32. The spectra show the partial DOS normalized by the number of atom (i.e., the units is 1/(eV atom)) to better visualize the states of the Co, Ni, and Li dopants. Grey areas represent the ZnO host states, whereas thick lines represent Co and Ni. Highest occupied energy is indicated by dashed vertical lines.

Thus, although Li co-doped $Zn_{1-x}M_xO$ has a local magnetic moment at the magnetic dopants, we find no FM phase in *bulk* $Zn_{1-x}M_xO$. Instead, we suggest that the observed enhancement of room temperature FM phase in *nanostructured* $Zn_{1-x}M_xO$ originates from the morphology of the nanorods. Theoretically, we find [6, 7] that Li-on-Zn in $Zn_{1-x}M_xO$ prefer energetically ($\approx$ 0.2 eV/Li) to be close to the M-on-Zn dopant, in order to locally depopulate the M 3*d*-states but also to compensate the M–O bonds. An explanation that Li co-

-doping stabilizes the $Zn_{1-x}M_xO$ nanorods is that when Li-on-Zn acceptors lower the Fermi level in $Zn_{1-x}M_xO$ to the same chemical potential as in pure ZnO, it is easier to grow rods with high morphology. This chemical-physical effect might be worth to study further.

5. Conclusion

This work discusses the morphology and magnetic coupling in nanostructured $Zn_{1-x}M_xO$ with Li as co-dopant, as presented in Ref. [6] for ZnO:Co and in Ref. [7] for ZnO:Ni. Experimentally, it is observed that low and moderate Li co-doping of the $Zn_{1-x}M_xO$ nanorod increases the rod morphology and enhances the room temperature FM phase. Theoretically, the main conclusions are: (i) Li-on-Zn prefer to be close to the magnetic Co- and Ni-on-Zn atoms to locally compensate the Co–O and Ni–O bonds, but also to locally depopulate the energetically highest Co and Ni 3*d*-states. (ii) The magnetic moment of Co and Ni in bulk $Zn_{1-x}M_xO$ is RKKY-like both without and with Li co-doping. Minor and moderate Li incorporation affects the local magnetic moment mainly via depopulation of the Co and Ni 3*d*-states. (iii) The total energies of FM and AFM phases are very comparable both without and with Li co-doping. Thus, the total energy calculations cannot explain room temperature FM phase, at least not with the present configurations of the magnetic Co and Ni elements.

Hence, for low and moderate Li concentrations, the Li-on-Zn acceptors do not induce a hole mediated FM phase in Li co-doped *bulk* $Zn_{1-x}M_xO$. Instead, the observed room temperature FM phase in Li co-doped $Zn_{1-x}M_xO$ *nanorods* can be explained by the better rod morphology in combination with ionization of the magnetic Co and Ni atoms. On further Li-on-Zn acceptor doping the ZnO host states are emptied at the valence-band maximum, however, these host-like holes enhance a stronger paramagnetic phase in $Zn_{1-x}M_xO$ rather than enhancing a FM phase.

Acknowledgments

C.P. acknowledges support from the Swedish Research Council, the Swedish Energy Agency, and the computers centers HPC2N and NSC through SNIC/SNAC.

References

[1] Ü. Özgür, Y.I. Alivov, C. Liu, A. Teke, M.A. Reshchikov, S. Dođan, V. Avrutin, S.-J. Cho, H. Morkoç, *J. Appl. Phys.* **98**, 041301 (2005).

[2] C. Klingshirn, *Phys. Status Solidi B* **244**, 3027 (2007).

[3] S.J. Pearton, C.R. Abernathy, M.E. Overberg, G.T. Thaler, D.P. Norton, N. Theodoropoulou, A.F. Hebard, Y.D. Park, F. Ren, J. Kim, L.A. Boatner, *J. Appl. Phys.* **93**, 1 (2003).

[4] T. Tietze, M. Gacic, G. Schütz, G. Jakob, S. Brück, E. Goering, *New J. Phys.* **10**, 055009 (2008).

[5] A. Zunger, S. Lany, H. Raebiger, *Physics* **3**, 53 (2010).

[6] O.D. Jayakumar, C. Sudakar, C. Persson, V. Sudarsan, T. Sakuntala, R. Naik, A.K. Tyagi, *Cryst. Growth Des.* **9**, 4450 (2009).

[7] O.D. Jayakumar, C. Sudakar, C. Persson, V. Sudarsan, R. Naik, A.K. Tyagi, *J. Phys. Chem. C* **114**, 17428 (2010).

[8] G. Kresse, D. Joubert, *Phys. Rev. B* **59**, 1758 (1999).

[9] C. Persson, C.L. Dong, L. Vayssieres, A. Augustsson, T. Schmitt, M. Mattesini, R. Ahuja, J. Nordgren, C.L. Chang, A. Ferreira da Silva, J.-H. Guo, *Microelectron. J.* **37**, 686 (2006).

[10] C. Persson, C. Platzer-Björkman, J. Malmström, T. Törndahl, M. Edoff, *Phys. Rev. Lett.* **97**, 146403 (2006).

[11] W.E. Pickett, S.C. Erwin, E.C. Ethridge, *Phys. Rev. B* **58**, 1201 (1998).

[12] T. Archer, R. Hanafin, S. Sanvito, *Phys. Rev. B* **78**, 014431 (2008).

[13] K. Sato, H. Katayama-Yoshida, *Jpn. J. Appl. Phys.* **39**, L555 (2000); *Phys. Status Solidi B* **229**, 673 (2002).